EIR-Bericht Nr. 428

EIR-Bericht Nr. 428

Eidg. Institut für Reaktorforschung Würenlingen
Schweiz

FINELM:
A Multigroup Finite Element Diffusion Code
Part II: R-Z Geometry and numerical accelerations

D. M. Davierwalla

Würenlingen, Mai 1981

EIR Bericht Nr. 428

FINELM: A Multigroup Finite Element Diffusion Code

Part II: R - Z Geometry and numerical accelerations

D.M. Davierwalla

May 1981

Abstract:

This is the second of a series of reports on FINELM, the E.I.R. finite element multigroup neutron diffusion code. Only the axisymmetric case in cylindrical coordinates is presented here. Furthermore, the numerical acceleration schemes incorporated viz. The Lebedev extrapolations and the coarse mesh rebalancing, space collapsing, are discussed. Examples which display the benifits of each of these schemes and their combination are presented.

Abstrakt:

In der Reihe der Berichte über FINELM, den "Finite element multigroup neutron diffusion code" des E.I.R., ist dies der zweite.

Nur der achsial-symmetische Fall in Zylinder Koordinaten wird dargelgt. Die eingebauten numerischen Beschleunigungsmethoden, nämlich die Lebeder Extrapolation und die "Coarse mesh rebalancing" werden diskutiert. Es werden Beispiele behandelt, die neben der Auswirkung der einzelnen Methoden auf die Konvergenz des Problems auch den Einfluss bei gleichzeitiger Anwendung zeigen.

Contents

Introduction

Enough has been said about the history of FINELM in reference (1). Here, we wish to restrict ourselves to only the R-Z geometry, the consequences and to the acceleration schemes used. As in the previous report a few benchmark computations are presented as validation of the code. They are fewer than before because there is a lack of suitably defined benchmark problems in this geometry. The R-Z geometry destroyed the rotational invariance of the T matrices used to compute the sources. This lead to a redesign of the iteration scheme which was slower. The incorporation of the rebalancing scheme also doubled the work done in a iteration which also increased the cost of an iteration. However, this makes the incorporation of both direct and adjoint solutions into one overlay acceptable. In retrospect it may be remarked that had the code been originally developed as an R-Z code the X-Y geometry would have been a by-product.

Problem Definition

The current trend at E.I.R. towards H.T.R. pebble-bed reactors made it imperative to extend our multigroup finite element diffusion code, FINELM, to handle, both, X-Y and R-Z geometries. Lagrangian elements of degrees one through four are offered. Dissections permit the problem size to be independant of core memory and dependant only on peripheral storage. The problem definition is identical with that defined in (1) and is repeated here only for the sake of completeness.

We consider a domain Ω with boundary $\partial\Omega$. The equation to be solved is the diffusion equation given by:

$$-\nabla.D_g(r)\nabla\phi_g(r)+\Sigma_g^R(r)\phi_g(r)=\sum_{\substack{g'=1\\g'\neq g}}^{IGM}\Sigma_{g'\to g}(r)\phi_{g'}(r)+\frac{1}{k_{eff}}\sum_{g'=1}^{IGM}\chi_{g'}(\nu\Sigma_f)_{g'}(r)\phi_{g'}(r) \quad 1.1$$

for $r\in\Omega$, g=1,2... IGM the total number of groups. The boundary conditions are given by:

$$\left.\begin{aligned}\phi_g(r) - f_g(r) &= 0 \qquad r\in\partial\Omega_D, \text{ (Dirichlet)} \quad 1.2a\\ \frac{\partial\phi_g(r)}{\partial n} + \hat{\beta}\phi_g(r) + q_g &= 0 \quad r\in\partial\Omega_C, \text{ (Cauchy)} \quad 1.2b\end{aligned}\right\}$$

Equation (1.1) is the multigroup eigenvalue problem with fission and up- and down-scattering.

Additionally, the solutions are required to satisfy

(a) $\phi_g(r)$ must be continuous in $\bar{\Omega}$, the closure of Ω.

(b) $D_g \frac{\partial \phi_g(r)}{\partial n}$, the neutron current must be continuous across material interfaces.

(c) $\phi_g(r) \geq 0$ for all $r \epsilon \Omega$.

Dirichlet conditions of Eq. (1.2a) simply imply that the k_{eff} problem be solved for a reduced number of degrees of freedom. Conditions (a) and (b) are not difficult to satisfy by polynomial approximations. However (c) cannot always be satisfied by polynomial approximations so that we should expect the flux to become negative, at least locally, in the approximate solution.

The variational formulation necessitates conversion to a self adjoint elliptic boundary value problem which in turn dictates power iterations. Hence Eq. (1.1) is rewritten as

$$-\nabla . D_g(r) \nabla \phi^{(n)}(r) + \Sigma_g^R(r) \phi_g^{(n)}(r) = \sum_{g'<g} \Sigma_{g' \to g}(r) \phi_{g'}^{(n)}(r) + \sum_{g':g} \Sigma_{g' \to g}(r) \phi_{g'}^{(n-1)}(r) + \left[\sum_{g'=1}^{IGM} \chi_{g'} (\nu \Sigma_f)_{g'}(r) \phi^{(n-1)}(r) \right] / k_{eff}^{(n-1)} \qquad (1.3)$$

for g=1,2,...IGM

or

$$-\nabla . D_g(r) \nabla \phi(r) + \Sigma_g(r) \phi_g(r) = Q_g(r) \qquad g=1,2,...IGM \qquad (1.4)$$

where $Q_g(r)$ is the combined source in group g due to up and down scattering and fission.

2. The Variational Method

The advantage of the variational method over residual methods is that the trial functions need satisfy essential boundary conditions only. Natural boundary conditions which occur at symmetry boundaries or at material interfaces are taken care of by the functional itself. Furthermore, boundary conditions of the Cauchy type may also be made natural by extending the element functional to include an extra term, a line integral along the sides of an element which lie on the part of the external boundary of the region on which Cauchy conditions are specified. As far as reactor physics is concerned this leaves only Dirichlet conditions as essential.

2.i The Trial Functions

As in the X-Y geometry case we triangulate the region and introduce simplex coordinates, defined by

$$S_2:\{(\xi_1,\xi_2):\xi_1,\xi_2\geq 0,\ \xi_1+\xi_2\leq 1\} \tag{2.1}$$

A third, dependant variable is added so that $\xi_1+\xi_2+\xi_3=1$. Bivariate polynomials in these variables, complete over an element are constructed as follows:

We defined recursively

$$P_m(\xi)=P_{m-1}(\xi)*(\mathrm{NProx}\xi-m+1)/m \tag{2.2}$$

with $P_0(\xi)=1$.

At each node, defined in the triple subscript notation, (i,j,k) we construct $\alpha_{ijk}(\xi_1,\xi_2,\xi_3)=P_i(\xi_1)P_j(\xi_2)P_k(\xi_3)$.

It is easily checked that the α_{ijk}'s constitute Lagrange node influence functions. By placing an appropriate number of nodes the continuity of the flux across material interfaces can be assured irrespective of the direction of the interfaces in space. This is achieved because the polynomials are so constructed that their degree is invariant with respect to rotations. The functional may then be written

$$J[u]=\sum_e J^e[u]=\sum_e \sum_{i=1}^{5} J_i^e[u] \tag{2.3}$$

where the superscript denotes a finite element and the element functional is now split into five instead of four parts.

3. The Functional in R-Z Geometry

In any orthogonal curvelinear coordinate system (x_1,x_2,x_3) we define elementary lengths ℓ_1, ℓ_2 and ℓ_3. These are related to the coordinates through the metric coefficients, h_1,h_2,h_3. An elementary volume $dV_3=\ell_1\ell_2\ell_3=h_1h_2h_3dx_1dx_2dx_3$. Specializing to cylindrical coordinates

$$dV_3=drrd\theta dz=h_1h_2h_3drd\theta dz.$$

Hence, $h_1=h_3=1$ and $h_2=r$.

$$\nabla\phi=\bar{a}_r\frac{\partial\theta}{r\partial r}+\bar{a}_\theta\frac{1}{r}\frac{\partial\phi}{\partial\theta}+\bar{a}_z\frac{\partial\phi}{\partial z}$$

where $\bar{a}_r$, $\bar{a}_\theta$ and $\bar{a}_z$ are unit vectors in the directions r,θ,z. All partials of unit vectors are zero except

$$\frac{\partial\bar{a}_r}{\partial\theta}=\bar{a}_\theta \quad \text{and} \quad \frac{\partial\bar{a}_\theta}{\partial\theta}=-\bar{a}_r$$

3.1 Leakage

Since the functional remains invariant in any coordinate system

$$J_1|u|=\frac{D}{2}\int_{V^e}(\nabla u,\nabla u)dV_3=\frac{D}{2}(2\pi)\int_{A^e} r\left(\frac{du}{dr}\right)^2+r\left(\frac{du}{dz}\right)^2\,drdz \qquad (3.1.1)$$

where A_e is the area of the element in the R-Z plane. Disregarding the factor 2π the result is analogous to the X-Y geometry except that we compute the first moment about the z-axis. It is easily checked that the Euler equation of (3.1) is

$$-\left(\frac{1}{r}\frac{\partial}{\partial r}(ru_r)+u_{rr}\right) \qquad (3.1.2)$$

The negative Laplacian of the axisymmetriccase in cylindrical coordinates.

Introducing the simplex coordinates (ξ_1,ξ_2,ξ_3) with $\xi_1+\xi_2+\xi_3=1$ a point within the triangle is represented by the triple (ξ_1,ξ_2,ξ_3) in a local coordinate system. If $(r_i,z_i)i=1,2,3$ represents the vertices of the triangle and (r,z) any point inside

$$r=r_1\xi_1+r_2\xi_2+r_3\xi_3 \qquad (3.1.3)$$

and

$$z=z_1\xi_1+z_2\xi_2+z_3\xi_3$$

The flux, ϕ, is expressed in terms of the point fluxes at the element nodes. Thus

$$\phi(\xi_1,\xi_2,\xi_3)=\sum_{i=0}^{N}\sum_{j=1}^{N-i}\alpha_{ijk}(\xi_1,\xi_2,\xi_3)\phi_{ijk}=\sum_{q=1}^{Nodel}\alpha_q(\xi_1,\xi_2,\xi_3)\phi_q \qquad (3.1.4)$$

where i+j+k=N, the degree of the approximating polynomial and Nodel is the number of nodes in the element. Inserting these into (3.1.1)and performing the variation as in reference (2), all details are omitted here,we get

$$\frac{\partial J_1^e}{\partial \phi_m}=D\sum_{j=1}^{3}\cot\theta_j\sum_{q=1}^{Nodel}\phi_q\frac{1}{2A}\int_A\left(\frac{\partial \alpha_m}{\partial \xi_{j+1}}-\frac{\partial \alpha_m}{\partial \xi_{j+2}}\right)\left(\frac{\partial \alpha_q}{\partial \xi_{j+1}}-\frac{\partial \alpha_q}{\partial \xi_{j+2}}\right)(r_1\xi_1+r_2\xi_2+r_3\xi_3)drdz \tag{3.1.5}$$

m=1, Nodel, θ_i i=1,2,3 are the angles of the triangle and the subscripts on the ξ's are computed cyclically. The left hand side of the equation represents the sum of moments of three matrices M_i, i=1,2,3 about the Z-axis. Thus the discrete negative Laplacian is represented by

$$2\pi D\sum_{j=1}^{3}\cot\theta_j\left(M_1^{(j)}r_1+M_2^{(j)}r_2+M_3^{(j)}r_3\right) \tag{3.1.6}$$

where the j is merely a superscript and where $M_i^{(2)}$ and $M_i^{(3)}$ are generated from $M_i^{(1)}$ by permutations as in reference (2).

Again it is noted that both row and column sums of the discrete Laplacian sum to zero to ensure the singularity of the composite matrix and enables the reference potential (Scalar flux) to be outside the element and posess any arbitrary value. Further the Laplacian depends only on the shape of the element and the distances of the vertices from the z-axis.

The results are displayed in Fig. (1).

3.2 The Removal Term

$$J_2^e = \frac{1}{2}\int_{V_3^e} \Sigma_e^R u^2 dV_3 \qquad (3.2.1)$$

After introducing cylindrical coordinates, transforming these to simplex coordinates, using the polynomial approximation for the flux and performing the variation with respect to a point flux ϕ_m there results

$$\frac{\partial J_2^e}{\partial \phi_m} = \frac{2\pi\Sigma^R}{2} \sum_{j=1}^{Nodel} \int_A \alpha_m(\xi_1,\xi_2,\xi_3)\alpha_j(\xi_1,\xi_2,\xi_2)(r_1\xi_1+r_2\xi_2+r_3\xi_3)\,drdz, \quad m=1\ Nodel \qquad (3.2.2)$$

This defines the sum of first moments about the Z-axis of three matrices and is denoted by:

$$T=T_1r_1 + T_2r_2 + T_3r_3 \qquad (3.2.3)$$

The sum of all the elements of the T_i matrices sum to unity. Note that the invariance with respect to rotations which permitted the separation of the graph theoretic structure of the matrix from the numerical energy dependant values which obtains in X-Y geometry does not carry over into R-Z geometry. The results are displayed in Fig. (2).

3.3 The Source Term (External)

As in the X-Y (see 1) case the external prescribed source G is expanded as a polynomial over the element and after performing the variation with respect to a point flux ϕ_m we arrive at

$$\frac{\partial J_3^e}{\partial \phi_m} = 2\pi \sum_{i=1}^{Nodel} G_i \left[\int_A (\alpha_m\alpha_j)(r_1\xi_1+r_2\xi_2+r_3\xi_3)\,drdz\right] \quad m=1,\ Nodel \qquad (3.3.1)$$

The results are similar to the removal term. The results are displayed in Fig. (2).

3.4 Cauchy Boundary Conditions

In the R-Z case we are forced to distinguish between boundary conditions prescribed on the top and bottom discs and those on the cylindrical surface. As before we consider a one-simplex

$$S_1:\{\xi_1;\ 0\leq\xi_1\leq 1\} \tag{3.4.1}$$

and introduce a slack or dependant variable such that $\xi_1+\xi_2=1$. Then the conditions on the discs lead to the functional

$$J_4^e[u]=\frac{1}{2}\beta\int_{V_2^e}u^2dV_2+\int_{V_2^e}qudV_2 \tag{3.4.2}$$

where V_2^e is the surface of the element on the disc and

$$\beta=\frac{1}{2.131338}\left(\frac{1-\text{Albedo}}{1+\text{Albedo}}\right) \tag{3.4.3}$$

Inserting the flux approximation and performing the variation with respect to the point fluxes yields

$$\frac{\partial J_4^e[\phi]}{\partial\phi_m}=\pi\sum_{j=1}^{N+1}\phi_j\int_{r_1}^{r_2}\beta\alpha_j\alpha_m rdr+2\pi\int_{r_1}^{r_2}q\alpha_m rdr \tag{3.4.4}$$

Here (N+1) are the number of nodes along the side of the element on the disc ie (NPROX+1), and

$$r=r_1\xi_1+r_2\xi_2 \tag{3.4.5}$$

The first term in Eq. (3.4.4) results in the sum of two first moments of matrices $(BCOEF)_1$ and $(BCOEF)_2$ about the z-axis, while the second is the sum of two moments of vectors $QCOEF_1$ and $QCOEF_2$ about the same axis.

Boundary conditions of the cylindrical surface yield the functional

$$J_5^e[u] = \pi r_2 \beta \int_{z_2}^{z_3} u^2 dz + 2\pi r_2 \int_{z_2}^{z_3} qudz$$

After performing the variation the first term yields moment of a single matrix, BCOEF, which is identical to the matrix from X-Y geometry. The second term is the moment of a single vector which (the vector) is identical to that from the X-Y geometry. In passing it may be noted that the matrix BCOEF is the sum of $(BCOEF)_1$ and $(BCOEF)_2$ and a similar statement applies to the vector QCOEF and $(QCOEF)_1$ and $(QCOEF)_2$. For the results consult Fig. (3).

Dirichlet Boundary Conditions

Since these are prescribed fluxes no variation is taken with respect to these fluxes and the final result is a reduction of the degrees of freedom. The situation is identical to that which obtains in X-Y geometry.

4. Chebyshev Acceleration

The Chebyshev acceleration (extrapolation) scheme is known to work well for systems of equation which have real and positive eigenvalues, a situation which is assured by the variational formulation.

If we denote by F, the iteration matrix of the system we have for the power method,

$$\phi^{(n+1)} = \frac{1}{k_{ekk}^{(n-1)}} F \phi^{(n)} \tag{4.1}$$

The extrapolation scheme used is:

$$\psi^{(n)} = \frac{1}{k_{eff}^{(n-1)}} \omega^{(n)} F\phi^{(n-1)} + (1-\omega^{(n)})\phi^{(n-1)} = \omega^{(n)}\phi^{(n)} + (1-\omega^{(n)})\phi^{(n-1)} \tag{4.2}$$

Here, the first term of the right hand side is actually $\omega^{(n)}\phi^{(n)}$, where $\phi^{(n)}$ is the flux which results as a solution at the n th iteration, and $\psi^{(n)}$ is the extrapolated flux at the end of the n th. iteration. The k_{eff} is computed from the fluxes prior to extrapolation, by the Rayleigh quotient. It is known that for hermetian symmetric matrices, the convergence rate of the Rayleigh quotient is twice as fast as that computed from the (production/distribution)-ratio, even through the latter may have more physical meaning.

Denote the true eigenvalues of F are by

$$0<\mu_N<\mu_{N-1} \cdots\cdots \mu_1<\mu_0 \tag{4.3}$$

and the eigenvectors by u_n, n=0,1,...N.

For matrices of large order μ_N may be taken to be zero and after an appropriate number of iterations the current k_{eff} is sufficiently close to μ_0.

We normalize the second largest eigenvalue to unity by introducing

$$\gamma_j = 2\left(\frac{\mu_j-\mu_N}{\mu_1-\mu_N}\right) - 1 \simeq 2\,\frac{\mu_j}{\mu_1} - 1 \qquad (4.4)$$

Hence, $-1 \leq \gamma_j \leq 1 \quad 1 \leq j \leq N \quad$ and $\gamma_0 > 1$

The initial flux guess may be expressed as a linear combination of the eigenvectors. Because the matrix is real and symmetric, the algebraic and the geometric multiplicity of an eigenvalue are equal and a full compliment of eigenvectors exist. We assume that the eigenvalue of maximum modulus N is unique. Hence,

$$\phi^{(0)} = \sum_{i=1}^{N} a_i^{(0)}\, u_i \qquad (4.5)$$

and a current solution $\phi^{(t)}$ as

$$\phi^{(n)} = \eta^{(n)}(\gamma_0)\; a_0^{(0)}\; u_0 + \sum_{i=1}^{N} \eta^{(n)}(\gamma_i)\; a_i^{(0)}\; \mu_i \qquad (4.6)$$

where $\eta^{(n)}(\gamma_i)$ is a n-th degree polynomial in γ_i defined by

$$\eta^{(n)}(\gamma_i) = \prod_{p=1}^{n} \left[\omega^{(p)} \frac{(\gamma_i+1)}{2k_{eff}^{(p-1)}}\, \mu_1 + 1 - \omega^{(p)}\right] \qquad (4.7)$$

We assume that $k_{eff}^{(p-1)}$ is sufficiently close to μ_0. Under these circumstances the above equation may be rewritten as

$$\eta^{(n)}(\gamma_i) = \prod_{p=1}^{n} \left[\omega^{(p)} \sigma \frac{\gamma_i + 1}{2} + 1 - \omega^{(p)} \right] \tag{4.8}$$

where σ is the dominance ratio $(\mu_1/\mu_0)<1$. In equation (4.6) the first term on the right hand side is the contribution from the fundamental mode and the second term is the sum of contributions of higher modes or residuals. Convergence, then, implies the reduction of the residuals to a sufficiently small acceptable magnitude for some n. The problem is then reduced to the minimization of

$$\max \left| \frac{\eta^{(k)}(\gamma_n)}{\eta^{(k)}(\gamma_0)} \right| \tag{4.9}$$

after a preselected number of iterations denoted by K. This means that a set of $\omega^{(j)}$'s have to be constructed for j=1,2,...K to minimize the ratio depicted in (4.9) - at the K th step. Since the eingenvalues, the μ_j's and the γ_j's defined by them are not individually known it is usual to assume a continuous spectrum for γ in $[-1, +1]$, and restate (4.9) as minimize

$$\max_{-1<\gamma<+1} \left| \frac{\eta^{(k)}(\gamma)}{\eta^{(k)}(\gamma_0)} \right| \tag{4.10}$$

The problem is a classical one and the result is to select $\eta^{(k)}(\gamma)$ to be a K th degree Chebyshev polynomial.

$$T_k(\gamma) = \cos(K \cos^{-1}\gamma) \tag{4.11}$$

whose j th root is given by

$$z_j = \cos\left(\frac{\pi(2j-1)}{2K}\right) \qquad j=1,2,...K \tag{4.12}$$

Hence, the parameters $\omega^{(j)}$ are determined as the solution to

$$\omega^{(j)} \sigma \frac{z_j+1}{2} + 1 - \omega^{(j)} = 0 \tag{4.13}$$

which yields

$$\omega^{(j)} = \frac{1}{1-(\frac{\sigma}{2})\left[\cos(\frac{\pi(2\gamma-1)}{2K}) + 1\right]} \tag{4.14}$$

The above method assumes that the dominance ratio is known. In practice σ has to be estimated during the run. We have

$$\phi^{(0)} = \sum_{i=0}^{N} a_i u_i \tag{4.15}$$

$$\phi^{(n)} = \sum_{i=0}^{N} a_i (\frac{\mu_i}{\mu_0})^n u_i = a_0 u_0 + \sum_{i=1}^{N} a_i (\frac{\mu_i}{\mu_0})^n u_i$$

$$\simeq \phi^{(\infty)} + a_1 (\frac{\mu_1}{\mu_0})^n u_1 \text{ assymptotically} \tag{4.16}$$

$$\frac{\phi^{(n)} - \phi^{(n-1)}}{\phi^{(n-1)} - \phi^{(n-2)}} = \frac{\sigma^{n-1}(\sigma-1)}{\sigma^{n-2}(\sigma-1)} = \sigma \tag{4.17}$$

The estimation is done by

$$\frac{< w, |\phi^{(n)} - \phi^{(n-1)}| >}{< w, |\phi^{(n-1)} - \phi^{(n-2)}| >}$$

where $$\sigma = \frac{< w, \text{error}^{(n)} >}{< w, \text{error}^{(n-1)} >} \tag{4.18}$$

and w is some weighting function. For $w=\bar{1}$, a vector of all one's,

$$\sigma = \frac{||\text{error}^{(n)}||_1}{||\text{error}^{(n-1)}||_1} \qquad (4.19)$$

This is the estimate used in the code. A better estimate, one that converges twice as fast is to use $w=\phi^{(n)}$. However, this requires the storage of two error vectors whereas in (4.19) we require the storage of only two scalars. There are two drawbacks of the one parameter Chebyshev method. If the cycle length is large some values of $\omega^{(t)}$ are large, so that $\omega^{(t)}$ and $1-\omega^{(t)}$ are similar in magnitude but have opposing sign. If the problem has almost converged $\phi^{(t)}$ is close to $\phi^{(t-1)}$ and the extrapolated flux $\psi^{(t)}= \omega^{(t)}\phi^{(t)}+(1-\omega^{(t)})\phi^{(t-1)}$ is determined largely by round off. Furthermore, the error is minimized at the end of K iterations. Hence it is a good practice to choose K reasonably small and use it cyclically. We found K=6 adequate.

Lebedev extrapolation (3), (4)

The Lebedev extrapolation used in FINELM is essentially a rearrangement of the single parameter Chebyshev extrapolation.

For a cycle length of six the Chebyshev sequence would give

$$\omega^{(t)} = \frac{1}{1-(\frac{\sigma}{2})\left[\cos(\frac{\pi}{12}m)+1\right]}$$

with $m^{(t)}=1,3,5,7,9,11$.
In the Lebedev case the sequence $m^{(t)}$ is rearranged to give

$$m^{(t)} = 3,9,5,7,1,11$$

The above cycle contains a subcycle of length two, so that it is quite possible to reach the convergence error criterion at the end of a subcycle.

4.1 Coarse Mesh Rebalancing

The Lebedev extrapolation worked well on all the benchmark problems that we had to date. Once, the nineteen group Proteus computations with strong upscatter, the Lebedev extrapolations introduced instability. If the extrapolations were switched off, the results converged, albeit slowly, with the rate dictated by the power iterations alone. This lead to the introduction of coarse mesh rebalancing. Both, space collapsing and group collapsing were tried out, but only the former retained. For a given right hand side the flux solution computed is exact due to the use of a direct solution method. The error in the $k_{eff}^{(n)}$ and the flux at the n-th iteration is due to errors in the fission and scatter sources. These errors come due to the use of delayed fluxes. The group collapsing method lead to rebalance within one or two iterations hence was abandoned.

4.2 Space Collapsing

Here, the idea is to reduce the region to a single point. For the sake of conciseness we consider a three group eigenvalue problem with both up and down scatter. The discretized problem may be depicted as

$$\begin{bmatrix} \underline{\underline{A}}_{11} & \underline{\underline{A}}_{21} & \underline{\underline{A}}_{13} \\ \underline{\underline{A}}_{21} & \underline{\underline{A}}_{22} & \underline{\underline{A}}_{23} \\ \underline{\underline{A}}_{31} & \underline{\underline{A}}_{32} & \underline{\underline{A}}_{33} \end{bmatrix} \begin{bmatrix} \phi_1 \\ \phi_2 \\ \phi_3 \end{bmatrix} = \frac{1}{k_{eff}} \begin{bmatrix} \chi_1 & \underline{\underline{F}}_{11} & \chi_1 & \underline{\underline{F}}_{22} & \chi_1 & \underline{\underline{F}}_{33} \\ \chi_2 & \underline{\underline{F}}_{11} & \chi_2 & \underline{\underline{F}}_{22} & \chi_2 & \underline{\underline{F}}_{33} \\ \chi_3 & \underline{\underline{F}}_{11} & \chi_3 & \underline{\underline{F}}_{22} & \chi_3 & \underline{\underline{F}}_{33} \end{bmatrix} \begin{bmatrix} \phi_1 \\ \phi_2 \\ \phi_3 \end{bmatrix} \tag{4.2.1}$$

The fluxes depicted are group fluxes and the overall matrices are partitioned into blocks according to groups. The matrices $\underline{\underline{F}}_{ii}$ are those constructed by using $\nu\Sigma_f$ for the i th group.

Matrix $\underline{\underline{A}}_{ii}$, incorporates the leakage, removal and boundary value components for the i th group. Equation (4.2.1) does not reflect the iteration scheme used. The actual computational scheme is:

$$\left.\begin{aligned}
\underline{\underline{A}}_{11}\phi_{g=1}^{(n)} &= \frac{\chi_1}{k_{eff}^{(n-1)}} \sum_{j=1}^{3} F_{jj}\phi_j^{(n-1)} + \underline{\underline{A}}_{12}\phi_2^{(n-1)} + \underline{\underline{A}}_{13}\phi_3^{(n-1)} \\
\underline{\underline{A}}_{22}\phi_{g=2}^{(n)} &= \frac{\chi_2}{k_{eff}^{(n-1)}} \sum_{j=1}^{3} F_{jj}\phi_j^{(n-1)} + \underline{\underline{A}}_{21}\phi_1^{(n)} + \underline{\underline{A}}_{23}\phi_3^{(n-1)} \\
\underline{\underline{A}}_{33}\phi_{g=3}^{(n)} &= \frac{\chi_3}{k_{eff}^{(n-1)}} \sum_{j=1}^{3} F_{jj}\phi_j^{(n-1)} + \underline{\underline{A}}_{31}\phi_1^{(n)} + \underline{\underline{A}}_{32}\phi_2^{(n)}
\end{aligned}\right\} \qquad (4.2.2)$$

and from the solution $k_{eff}^{(n)}$ is determined. The use of delayed fluxes introduces errors in the group fluxes and the error propagates down through the various groups. Thus even in the last, the third, group even the down scatter terms are not error free because the fluxes ϕ_1 and ϕ_2 were not error free. To remedy this, the following recipe is used. At the end of the n-th iteration $k_{eff}^{(n)}$ and $\phi_i^{(n)}$, i=1,2,3 are known. We denote by

$$I'_{ij} = \int_{r\epsilon\bar{\Omega}(r)} (\text{Leakage+Removal+Boundary})_i(r)\phi_j^{(n)}(r)dr$$

and (4.2.3)

$$M'_{ii} = \int_{r\epsilon\bar{\Omega}(r)} \nu\Sigma_f(r)_i\phi_i^{(n)}(r)dr$$

where the leakage, removal, boundary and the production operators are integrated over the closure of the domain. Since the discretized scheme may contain an arbitrary number

of points only the crudest spatial integration scheme may be used. We used the trapezoidal rule neglecting the halving of the values at the boundaries of the spatial blocks. This leads to the redefinition of Fq. (4.2.3) as

$$I_{im}^{g=i} = \sum_{k,j=1}^{N} (a_{kj})\ \phi_j^{g=m}$$

and (4.2.4)

$$M_{ii}^{g=i} = \sum_{k,j=1}^{N} (f_{kj})\ \phi_j^{g=i}$$

where the fluxes that are used are those at the end of the n-th iteration, where j and k run over the points in space and $I_{im}^{g=i}$ and $M_{ii}^{g=i}$ are scalars. This leads to:

$$\begin{pmatrix} I_{11} & I_{12} & I_{13} \\ I_{21} & I_{22} & I_{23} \\ I_{31} & I_{32} & I_{33} \end{pmatrix} \begin{pmatrix} c_1^{(n)} \\ c_2^{(n)} \\ c_3^{(n)} \end{pmatrix} = \frac{1}{k_{eff}^{(n)}} \begin{pmatrix} \chi_1 M_{11} + \chi_1 M_{22} + \chi_1 M_{33} \\ \chi_2 M_{11} + \chi_2 M_{22} + \chi_2 M_{33} \\ \chi_3 M_{11} + \chi_3 M_{22} + \chi_3 M_{33} \end{pmatrix}$$

(4.2.5)

The solution determines the coefficients $c_g^{(n)}$ with which the fluxes are weighted. Balance is achieved when all the $c_g^{(n)}$ are unity. Once all the $c_g^{(n)}$'s are unity the system is in balance and from this point onwards the convergence is that solely due to the power iterations. In the 19 group Proteus case mentioned previously, which is about the most difficult case, we have handled,it required about 10 iterations for the system to come into balance, after which the convergence is slow.

4.3 The actual scheme used

The scheme used is as follows:

a) We determine the $\phi_g^{(n)}(r)$'s and from them the $k_{eff}^{(n)}$

b) We use the coarse mesh rebalancing alone till a sufficiently accurate estimate of the dominance ratio has been achieved. Thereafter, the σ is kept fixed and the procedure is changed to

a')Determine the $\phi_g^{(n)}(r)$'s and the $k_{eff}^{(n)}$ as in (a)

b')Extrapolate the fluxes by the Lebedev method

c) Determine and apply the group weights.

This scheme has worked well since April 1979. We have in sections 4.1 and 4.2 only considered the direct solution. Due to the fact that the adjoint solution also has to be computed we do not use $\chi_g/k_{eff}^{(n)}$ as the fission source in Eq. (4.2.5).

5. Current Capabilities of the Code

The current capabilities and highlights of the code are summerized here as a matter of general interest.

1) X-Y and R-Z geometries are offered. R-θ will become available in the very near future

2) Direct and adjoint solutions are available

3) Triangular and rectangular Lagrangian elements or a mixture of the two may be chosen. It is recommended, however, that tringular elements be used when symmetry boundaries may be exploited or when material interfaces do not run parallel to the coordinate axes.

4) Degrees of approximation, one through four are available. The introduction of general degree subroutines will extend this range. A practical bound on the maximum degree of approximation, dictated by the word length of the computer is about eight or so.

5) The solution is by a variable band Choleski decomposition.

6) Cuts may be specified by the user in order to run the problem in reduced core. It should be brought to the users attention that cuts introduce no numerical approximation. They merely sequence partial problems. The size of the problem that can be handled is limited only by peripheral storage which is virtually unlimited.

7) The acceleration method used in the outer iteration is the Lebedev extrapolation with coarse mesh rebalancing - space collapsing.

8) A restart option is available.

9) A very efficient input subroutine, requiring a minimum of key punch effort has been provided by C.E. Higgs.

10) Both external source problems and k_{eff} problems may be solved.

Conclusion and Recommendations

Till now, the single parameter extrapolation has sufficed. If it is necessary to go over to a two parameter Chebyshev method, or its Lebedev variation the dominance ratio should be estimated by using $w=\phi^{(n)}$ in (4.19). There is also every indication that R-θ geometry will adversely effect packing density. This may be remedied by applying renumbering algorithms to the section graphs.

$6*M_3^{(1)}$=0/0,1/0,-1,1/ with $M_1^{(1)}=M_2^{(1)}=M_3^{(1)}$

P = (1,2,3)

Linear Approximation

$30*M_1^{(1)}$=0/0,3/0,1,3/0,-2,2,24/0,-4,-4,0,8/0,2,-2,-24,0,24/

$30*M_2^{(1)}$=0/0,9/0,2,3/0,3,1,8/0,-11,-5,-4,16/0,-3,-1,-8,4,8/

$30*M_3^{(1)}$=0/0,3/0,2,9/0,-1,-3,8/0,-5,-11,4,16/0,1,3,-8,-4,8/

P = (1,2,3)(4,5,6)

Quadratic Approximation

$3360*M_1^{(1)}$=0/0,200/0,-38,200/0,198,-198,4373/0,-234,-90,-972,2430/
0,-324,162,0,162,810/0,162,-324,0,162,-648,810/
0,-90,-234,972,486,162,162,2430/0,-198,198,-4374,972,
0,0,-972,4374/0,324,324,0,-2916,-324,-324,0,-2916,
5832/

$3360*M_2^{(1)}$=0/0,1028/0,-128,200/0,-117,-45,648/0,477,-153,81,2430/
0,-1503,369,81,-648,3078/0,603,-441,81,324,-1944,1782/
0,117,-117,243,324,-486,486,810/0,117,45,-648,-81,-81,
-81,-243,648/0,-594,270,-324,-2754,1134,-810,-1134,324,
3888/

$3360*M_3^{(1)}$=0/0,200/0,-128,1028/0,45,117,648/0,-117,117,-243,810/
0,-441,603,-81,486,1782/0,369,-1503,-81,-486,-1944,3078/
0,-153,477,-81,324,-648,2430/0,-45,-117,-648,243,81
81,81,648/0,270,-594,324,-1134,-810,1134,-2754,-324,
3888/

P = (1,2,3)(4,5,6)(5,7,9)

Cubic Approximation

$Q_1 = (M_1^{(1)} r_1 + M_2^{(1)} r_2 + M_3^{(1)} r_3)$

$Q_{i+1} = (P^i) Q_1 (P^i)^T$

Fig. (1): The lower triangular part of the Q_i matrices used to construct the negative Laplacian of an element

$120*T_1$=6/2,2/2,1,2/

$120*T_2$=2/2,6/1,2,2/

$120*T_3$=2/1,2/2,2,6/

P = (1,2,3)

Linear Approximation

$2520*T_1$=30/-4,6/-4,1,6/12,-8,-12,96/-4,-4,-4,32,32/12,-12,-8,48,32,96/

$2520*T_2$=6/-4,30/1,-4,6/-8,12,-12,96/-12,12,-8,48,96/-4,-4,-4,32,32,32/

$2520*T_3$=6/1,6/-4,-4,30/-4,-4,-4,32/-12,-8,12,32,96/-8,-12,12,32,48,96/

P = (1,2,3)(4,5,6)

Quadratic Approximation

$13440*T_1$=60/5,8/5,1,8/36,15,21,324/-18,-12,3,81,162/3,-6,3,-27,54,54/
3,3,-6,-27,-27,-27,54/-18,3,-12,-81,0,-27,54,162/36,21,15
162,-81,-27,-27,-81,324/0,18,18,162,0,0,0,0,162,648/

$13440*T_2$=8/5,60/1,5,8/-12,-18,3,162/15,36,21,-81,324/21,26,15,-81,162,324/
3,-18,-12,0,-81,-81,162/3,3,-6,-27,-27,-27,54,54/-6,3,3,54,-27,
-27,-27,-27,54/18,0,18,0,162,162,0,0,0,648/

$13440*T_3$=8/1,8/5,5,60/-6,3,3,54/3,-6,3,-27,54/3,-12,-18,-27,54,162/
21,15,36,-27,-27,-81,324/15,21,36,-27,-27,-27,-81,162,324/-12,3,-18,
54,-27,0,-81,-81,162/18,18,0,0,0,0,162,162,0,648/

P = (1,2,3)(4,6,8)5,7,9)

Cubic Approximation

$$T^e = T_1 r_1 + T_2 r_2 + T_3 r_3$$

NB $(P^i)(T^e)(P^i)^T \nmid T^e$

Fig. (2): The lower triangular part of the T^e matrices used to construct external source, fission, scattering and removal terms for an element

```
12*BCOEF1=3/1,1/0,0,0/
12*BCOEF2=1/1,3/0,0,0/

6*QCOEF1=-3,-3,0
6*QCOEF2=-1,-2,0
```

Linear Approximation

```
60*BCOEF1=8/-2,8/0,0,0/4,4,0,32/0,0,0,0,0/0,0,0,0,0,0/
60*BCOEF2=1/-1,7/0,0,0/0,4,0,16/0,0,0,0,0/0,0,0,0,0,0/

6*QCOEF1=-1,0,0,-2,0,0.
6*QCOEF2=0,-1,0,-2,0,0.
```

Quadratic Approximation

```
3360*BCOEF1=237/19,19/0,0,0/189,9,0,891/-81,9,0,-81,405/
3360*BCOEF2=19/19,237/0,0,0/9,-81,0,405/9,189,0,-81,891/

120*QCOEF1=-13,-2,0,-36,-9,0,0,0,0,0.
120*QCOEF2=-2,-13,0,-9,-36,0,0,0,0,0.
```

Cubic Approximation

$(CB)^e$ = beta*(r_1*BCOEF1+r_2*BCOEF2)*L_3

$(CV)^e$ = QU(r_1*QCOEF1+r_2*QCOEF2)*L_3

Fig. (3): $(CB)^e$, the contribution to the element matrix and $(CV)^e$ the contribution to the element vector for Cauchy Boundary conditions $D\frac{\partial \phi}{\partial n} + \beta\phi + q = 0$ prescribed on a disc

```
12*BCOEF=4/2,4/0,0,0/

 6*QCOEF=-4,-5,0
```

Linear Approximation

```
60*BCOEF=9/-3,15/0,0,0/4,8,0,48/0,0,0,0,0/0,0,0,0,0,0/

 6*QCOEF=-1,-1,0,-4,0,0
```

Quadratic Approximation

```
3360*BCOEF=256/38,256/0,0,0/198,-72,0,1296/-72,198,0,-162,1296/

120*QCOEF=-15,-15,0,-45,-45,0,0,0,0,0
```

Cubic Approximation

$(CB)^e$ = Beta*r_2*(BCOEFF)*L_1

$(CV)^e$ = QU*r_2(QCOEF)*L_1

Fig. (4): $(CB)^e$, the contribution to the element matrix and $(CV)^e$ the contribution to the element vector for Cauchy boundary conditions $D\frac{\partial \phi}{\partial n} + \beta\phi + q = 0$ prescribed on the cylindrical surface

Some Benchmark Problems

Example 1 (6)

This was selected from the Argonne National Laboratory benchmark problem book ANL-7416. The problem with identification number 8, was submitted in January 1973 by H.L. Dodds Jr. (U. of Tenn.), adopted in June 1977 by E.L. Fuller (E.P.R.I.) and W. Werner (GRS-München) and has as a descriptive title: Two dimensional (R-Z) reactor model.

The composition of the reactor is displayed in Fig. (5) and the cross-sections in Fig. (6). The suggested function of the problem is to test two dimensional neutron kinetics. We have used it for only computing the initial k_{eff}. The benchmark book presents two distinct solutions all using finite difference codes with common step sizes in the radial and axial directions.

The first solution presented by Savannah River Laboratory, Jan. 1973, is computed using single precision, on an IBM-360, Model 195 machine with the code TWODTA.

The second solution is presented by Chalk River Nuclear laboratories with the code ADEP utilizing an alternating direction explicit method with exponential transformations.

We also present the results computed with FEM2D, the finite element code from the Institut für Kernenergetik und Energiesysteme, University of Stuttgart by courtsey of Prof. F.A.R. Schmidt.

The above and the FINELM solutions are displayed in Table (1).

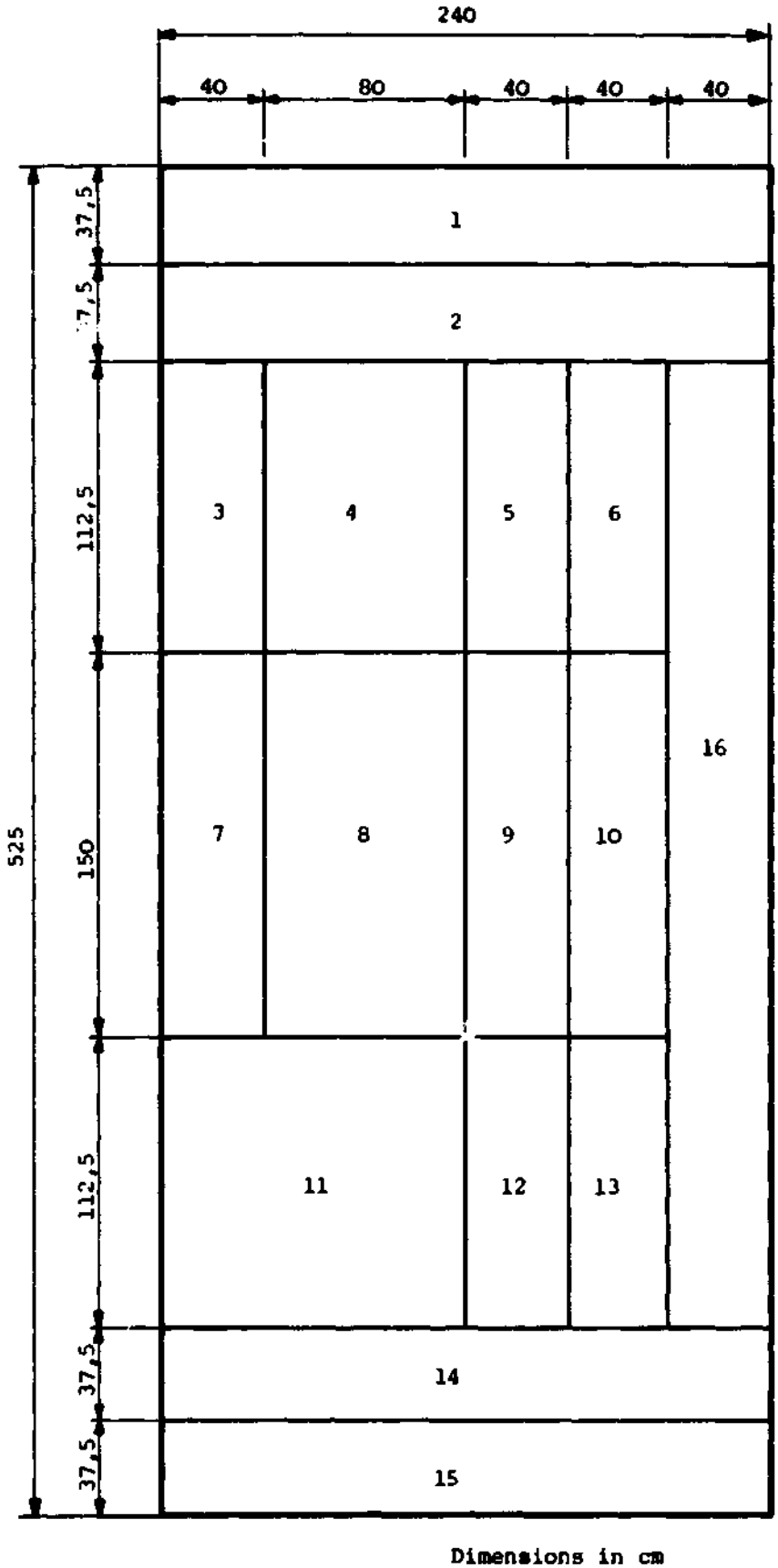

Fig. (5) 2D - (R-Z) Reactor Model
Argonne Code Center ANL-7416
Benchmark Problem ID. Nr. 8

Data:

Initial Two-Group Constants

Material	Region	Group i	D_i (cm)	$\Sigma_i^*(cm^{-1})$	$\nu\Sigma_{fi}(cm^{-1})$	$\Sigma_{1+2}(cm^{-1})$
1	1,15	1	1.0684+0	2.8-2	0	2.6-2
		2	0.32051+0	3.3-3	0	-
2	2,14	1	1.3495+0	1.201-2	0	1.2-2
		2	8.7032-1	1.9-2	0	-
3	3,4,11	1	1.3052+0	1.0475-2	1.1776-3	8.0351-3
		2	8.8857-1	1.3063-2	1.3268-2	-
4	5,12	1	1.3052+0	1.0475-2	1.1776-3	8.0351-3
		2	8.8857-1	1.2623-2	1.3268-2	-
5	6,13	1	1.3052+0	1.0475-2	1.1776-3	8.0351-3
		2	8.8857-1	1.2183-2	1.3268-2	-
6	7,8	1	1.3052+0	1.0475-2	1.1776-3	8.0351-3
		2	8.8857-1	1.3453-2	1.3268-2	-
7	9	1	1.3052+0	1.0475-2	1.1776-3	8.0351-3
		2	8.8857-1	1.2973-2	1.3268-2	-
8	10	1	1.3052+0	1.0475-2	1.1776-3	8.0351-3
		2	8.8857-1	1.2933-2	1.3268-2	-
9	16	1	1.2997+0	1.0470-2	1.2875-3	7.9061-3
		2	8.7951-1	1.3065-2	1.4246-2	-

$\chi_1 = 1 \quad \chi_2 = 0$

Cross section data for Argonne R-Z
Benchmark problem ID-8-AI.

Fig. (6)

Table (1)

Code	Type	Machine	Lab.	Computed Initial keff	Remarks
TWODTA	Finite Difference	IBM 360/195	Savannah River S.C. USA	.867053	ΔR=8cm ΔZ=18.75cm
ADEP	Finite Difference	CDC6600	Chalk River Canada	.866861	ΔR=8cm ΔZ=18.75cm
Diff2D	Finite Difference	CDC6400	EIR Switzerland	.867101	ΔR=8cm ΔZ=18.75cm, 20 Iterat
Diff2D	-	CDC174	EIR Switzerland	.86769	ΔR=8cm ΔZ=18.75cm, 39 Iterat
FEM-2D	Finite Element	CDC6600	IKE Stuttgart	.86690	Quadratic approximation
FEM-2D	Finite Element	CDC6600	IKE Stuttgart	.86711	Quadratic elements, more acc computation
FINELM	Finite Element	CDC6400	EIR Switzerland	.86735	84 Triangular elements. Quad Approx. 34 Iterations, k_{eff} ce 4E-6 Max flux dev. 2E-4
FINELM	Finite Element	CDC6400	EIR Switzerland	.8673011	84 Triangles.Quadratic Appro Iterations k_{eff} convergence Max flux dev. 5.4E-9
FINELM	Finite Element	CDC6400	EIR Switzerland	.86717	42 Rectangles.Quadratic Appr Iterations keff 4E-6 Max flu
FINELM	Finite Element	CDC6400	EIR Switzerland	.86718	42 Rectangles 4 th Order. 78 keff convergence 2.8E-9 Max 1.3E-7

Example 2.

As simple example we chose a bare homogeneous two group cylindrical reactor of total height 96 cm and radius 48 cm. The boundary conditions imposed were zero flux on the top and bottom discs as well as on the cylindrical surface. The cross sections used are given below in Table (2).

Cross section	Group 1	Group 2
D_g	2.68000451313	1.57876722277
Σ^R_g	5.457703768091E-2	1.449608761E-2
$\nu\Sigma^g_f$	3.0834481E-2	2.521E-2
$\Sigma_{g\to g'}$	-	4.079207068311E-2
χ_g	.575	.425

Table (2)

The analytic solution for k_{eff} is given by

$$k_{eff}=\frac{\chi_1\Sigma_{21}\nu\Sigma_{f2}}{(D_1B^2+\Sigma_1^R)(D_2B^2+\Sigma_2^R)}+\frac{\chi_2\nu\Sigma_{f2}}{(D_2B^2+\Sigma_2^R)}+\frac{\chi_1\nu\Sigma_{f1}}{(D_1B^2+\Sigma_1^R)}=1.265260034$$

where $B^2=(\frac{\pi}{H})^2+(\frac{\nu_0}{R})^2$ and H is the total height, R the maximum radius and ν_0 the first zero of $J_0(r)$. Both, the radius and the half-height were divided into six equal intervals resulting in a total of thirty six, 8 cm x 8 cm rectangular elements in the R-Z plane. The results for linear, quadratic, cubic and fourth order approximations are displayed in Tables 3,4,5 and 6.
In all cases the stopping criteria demanded an error of less than 1E-5 on the k_{eff} and an RMS flux error of less than 1.E-4.

Iteration Number	k_{eff}	k_{eff} error	Max.Rel.Point Flux deviation
1	2.000578	5.00E-1	-5.85E+0
2	1.332267	5.02E-1	-1.10E+0
3	1.306932	1.94E-2	-4.70E-1
4	1.287940	1.47E-2	-2.17E-1
5	1.276640	8.85E-3	-1.06E-1
10	1.263670	3.22E-5	-5.32E-4
11	1.263627	3.42E-5	-3.96E-5
16	1.263625	9.11E-9	-3.53E-7

Four iterations were required to estimate the dominance ratio $\sigma \simeq .5229 + .026$. A six cycle Lebedev extrapolation with coarse mesh rebalancing was used.

Table (3) Bare Homogeneous reactor 36 Linear rectangular elements

Iteration Number	k_{eff}	k_{eff} error	Max.Rel.Point Flux deviation
1	1.956195	4.89E-1	-1.16E+1
2	1.322131	4.80E-1	-2.21E+0
3	1.303545	1.43E-2	-7.28E-1
4	1.287569	1.24E-2	-2.94E-1
5	1.277461	7.91E-3	-1.37E-1
6	1.271671	4.55E-3	-6.90E-2
11	1.264924	1.61E-5	-3.98E-4
12	1.264902	1.81E-5	-2.82E-5
17	1.264901	2.93E-9	-2.80E-7

Five iterations were required to estimate the dominance ratio $\sigma=.5415\pm.027$. A six cycle Lebedev extrapolation with coarse mesh rebalancing was used

Table (4) Bare Homogeneous reactor 36 quadratic rectangular elements

Iteration Number	k_{eff}	k_{eff} error	Max.Rel.Point Flux deviation
1	1.934462	4.83E-1	-2.04E+1
2	1.318210	4.67E-1	-3.013E+0
3	1.301011	1.32E-2	-7.90E-1
4	1.286065	1.16E-2	-3.01E-1
5	1.276607	7.41E-3	-1.39E-1
6	1.271197	4.26E-3	-6.94E-2
11	1.264927	1.45E-5	-4.05E-4
12	1.264907	1.61E-5	-2.95E-5
17	1.264907	1.90E-9	-2.98E-7

Five iterations were required to estimate the dominance ratio σ=.5401$\pm$.027. A six cycle Lebedev extrapolation with coarse mesh rebalancing was used

Table (5) Bare Homogeneous reactor 36 cubic reactangular elements

Iteration Number	k_{eff}	k_{eff} error	Max.Rel.Point Flux deviation
1	1.930750	4.82E-1	-3.03E+1
2	1.316341	4.67E-1	-3.66E+0
3	1.300033	1.25E-2	-8.43E-1
4	1.285525	1.13E-2	-3.10E-1
5	1.276305	7.22E-3	-1.41E-1
6	1.271029	4.15E-3	-7.04E-2
11	1.264926	1.38E-5	-4.12E-4

Five iterations were required to estimate the dominance ratio σ=.5395$\pm$.027. A six cycle Lebedev extrapolation with coarse mesh rebalancing was used

Table (6) Bare Homogeneous reactor 36 fourth order reactangular elements

Four to five iterations are required to estimate the dominance ratio, $\sigma=\lambda_1/\lambda_2$. During this time only the coarse mesh rebalancing is active. Thereafter, both the six-cycle Lebedev extrapolation and the rebalancing are active. The tables display all the iterations, prior to the activation of the Lebedev extrapolations and only the first and sixth (the last) iteration of a particular Lebedev cycle.

Example 3

This example is not a benchmark problem. It was chosen, however, to illustrate the effect of the acceleration techniques. Fig. (7) depicts a simplified sketch of the Proteus experiment. The division into elements and materials is indicated in the diagram. The problem boils down to the computation of a nineteen group three material, k_{eff} problem in R-Z geometry. Linear approximations were used in order to keep costs low since the example is included for illustrative purposes only. The cross sections are displayed in Tables (7), (8), (9). The homogenized LEU2 cell corresponds to material 1, LEU2+ Aluminium to material 2 and the Reflector to material 3. As the tables are prints out from our RSYST data system a word of explanation is perhaps not superfluous. Spalte implies column and Zeilen rows. Thus the statement: "Zeilen 24 bis 35 sind gleich", indicates that rows 24 to 35 both inclusive are identical.

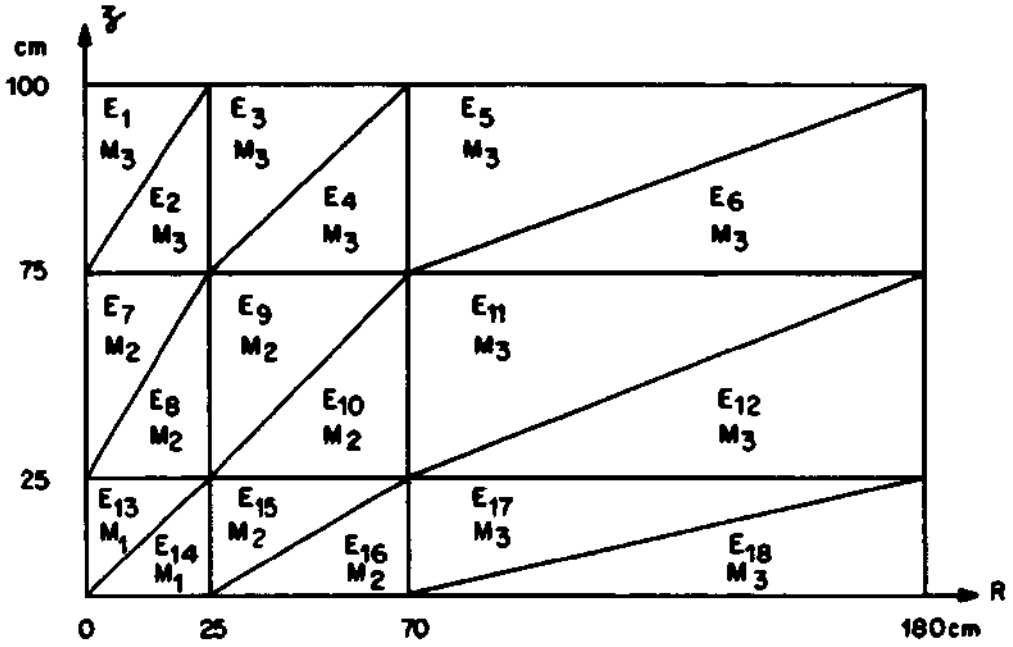

Fig.(7) A simplified model for the Proteus 19 Group case

4080520 HTR LEU2 ZELLE HOMOGENISIERT 19 68. 80GK 03.11.80

IMM= 35 IGM= 19 IMT= 5 IMS= 17 K1(5)= 0 K1(6)= 0 K1(7)= 665 K1(8)= 06772057116014525034

K1(9)= 0. K1(10)= 0 L1= 296

	SPALTE 1	SPALTE 2	SPALTE 3	SPALTE 4	SPALTE 5	SPALTE 6	SPALTE 7	SPALTE 8	SPALTE 9	SPALTE 10
1	3.72280E-05	1.91584E-05	1.13515E-04	3.68744E-04	3.36179E-04	4.39684E-04	5.32090E-04	3.99492E-04	1.78093E-04	1.40750E-04
2	1.21719E-01	2.19007E-01	2.33108E-01	2.34364E-01	2.38108E-01	2.37574E-01	2.31868E-01	2.36620E-01	2.32117E-01	2.32288E-01
3	6.67210E-05	8.50674E-05	7.28868E-04	1.84766E-03	3.69305E-03	5.49617E-03	1.02292E-03	5.82951E-03	4.97723E-04	3.45561E-04
4	1.02386E-04	4.81956E-05	2.86059E-04	9.39840E-04	8.28783E-04	1.10172E-03	1.40846E-03	1.03086E-03	4.44793E-04	3.58032E-04
5	1.36691E-01	2.33810E-01	2.46765E-01	2.47996E-01	2.51017E-01	2.51184E-01	2.45494E-01	2.50223E-01	2.45877E-01	2.46249E-01
6	0.	0.	0.	0.	0.	0.	0.	0.	0.	1.11658E-03
7	0.	0.	0.	0.	0.	0.	0.	0.	0.	0.
ZEILEN 7 BIS 13 SIND GLEICH										
14	0.	0.	0.	0.	0.	0.	0.	0.	0.	1.01033E-10
15	0.	0.	0.	0.	0.	0.	0.	0.	0.	3.21879E-06
16	0.	0.	0.	0.	0.	0.	0.	0.	1.11658E-03	5.53952E-03
17	1.29029E-01	2.25571E-01	2.36183E-01	1.68872E-01	1.72193E-01	1.70861E-01	1.67402E-01	2.07206E-01	1.71695E-01	1.84144E-01
18	0.	1.15948E-02	8.15343E-03	9.85289E-03	7.72267E-02	7.59310E-02	7.48327E-02	7.70692E-02	3.71269E-02	7.35943E-02
19	0.	0.	2.15235E-08	5.98652E-10	0.	0.	0.	0.	0.	0.
20	0.	0.	0.	0.	3.63019E-10	0.	0.	0.	0.	0.
21	0.	0.	0.	0.	0.	2.80015E-10	0.	0.	0.	0.
22	0.	0.	0.	0.	0.	0.	1.33443E-10	0.	0.	0.
23	0.	0.	0.	0.	0.	0.	0.	1.30026E-10	0.	0.
24	0.	0.	0.	0.	0.	0.	0.	0.	0.	0.
ZEILEN 24 BIS 35 SIND GLEICH										

	SPALTE 11	SPALTE 12	SPALTE 13	SPALTE 14	SPALTE 15	SPALTE 16	SPALTE 17	SPALTE 18	SPALTE 19	SPALTE
1	4.97166E-04	7.88349E-04	2.91509E-03	5.66571E-03	4.39486E-03	2.52904E-03	2.49905E-03	3.43412E-03	6.36091E-03	
2	2.41072E-01	2.34723E-01	2.38793E-01	2.43590E-01	2.42346E-01	2.41463E-01	2.47126E-01	2.64754E-01	3.00508E-01	
3	8.42880E-03	1.22759E-03	4.60738E-03	9.15113E-03	6.96121E-05	3.78467E-03	3.52032E-03	4.67392E-03	8.52986E-03	
4	1.22972E-03	1.90193E-03	7.96684E-03	1.57682E-02	1.21138E-02	6.72547E-03	6.46696E-03	8.78347E-03	1.61745E-02	
5	2.54802E-01	2.47592E-01	2.91100E-01	2.55490E-01	2.53774E-01	2.51522E-01	2.54578E-01	2.64619E-01	2.77194E-01	
6	3.93932E-03	3.58677E-03	2.70301E-02	4.57109E-02	3.78975E-02	2.83345E-02	3.72843E-02	3.95397E-02	4.12374E-02	
7	0.	0.	0.	0.	0.	0.	0.	0.	0.	
ZEILEN 7 BIS 9 SIND GLEICH										
10	0.	4.42755E-06	0.	0.	0.	0.	0.	0.	0.	
11	0.	1.51644E-05	5.59136E-05	0.	0.	0.	0.	0.	0.	
12	3.80793E-09	6.09611E-05	1.30959E-04	1.00231E-04	0.	0.	0.	0.	0.	
13	3.76850E-08	3.86823E-04	5.20070E-04	2.54961E-04	5.74899E-04	0.	0.	0.	0.	
14	1.47480E-07	2.20093E-03	3.00543E-03	1.08694E-03	1.51436E-03	4.95712E-03	0.	0.	0.	
15	9.97358E-07	6.34109E-03	1.29024E-02	4.44068E-03	3.99728E-03	8.37346E-03	8.61161E-03	0.	0.	
16	3.58355E-03	2.70291E-02	3.93696E-02	2.27941E-02	2.05016E-02	3.16190E-02	2.52507E-02	2.69482E-02	0.	
17	1.51549E-01	1.93785E-01	1.35193E-01	1.06054E-01	1.34958E-01	1.78146E-01	1.85654E-01	2.16928E-01	2.27390E-01	
18	5.46613E-02	8.79159E-02	3.22190E-02	3.40118E-02	5.40536E-02	5.72059E-02	3.10866E-02	2.55801E-02	7.47657E-03	
19	9.02275E-05	5.98236E-03	7.15320E-04	7.31371E-03	2.76052E-02	3.06896E-02	1.16708E-02	8.68661E-03	2.58929E-03	
20	0.	7.19299E-08	0.	9.17310E-05	5.90674E-03	1.84484E-02	7.73746E-03	4.58143E-03	1.48379E-03	
21	0.	0.	0.	0.	6.17904E-05	2.95684E-03	3.24486E-03	1.87976E-03	4.99240E-04	
22	0.	0.	0.	0.	0.	0.	4.71953E-04	8.55990E-04	2.13670E-04	
23	0.	0.	0.	0.	0.	0.	0.	1.20972E-04	1.02489E-04	
24	0.	0.	0.	0.	0.	0.	0.	0.	3.14698E-06	
25	0.	0.	0.	0.	0.	0.	0.	0.	0.	
ZEILEN 25 BIS 35 SIND GLEICH										

Table (7) HTR Leu 2 Cell, homogenized - Material 1

4G36300 HTR LEU2 + ALUMINIUM 03.11.80

INH= 35 IGM= 19 IHT= 5 IHS= 17 M1(5)= 0 M1(6)= 0 M1(7)= 665 M1(8)= 13714002431020640443

M1(9)= 0. M1(10)= 0 L1= 280

	SPALTE 1	SPALTE 2	SPALTE 3	SPALTE 4	SPALTE 5	SPALTE 6	SPALTE 7	SPALTE 8	SPALTE 9
1	3.28854E-05	1.69214E-05	1.02451E-04	3.21882E-04	2.90116E-04	3.87166E-04	4.65095E-04	3.44442E-04	1.56894E-04
2	1.08473E-01	1.94897E-01	2.07176E-01	2.08848E-01	2.18593E-01	2.12544E-01	2.05339E-01	2.09047E-01	2.05516E-01
3	5.97454E-05	7.83023E-05	5.84860E-04	1.39623E-03	2.64883E-03	3.82541E-03	8.91059E-04	4.00068E-03	4.42863E-04
4	9.04426E-03	4.25442E-05	2.57997E-04	8.21015E-04	7.15558E-04	9.68015E-04	1.23183E-03	8.89138E-04	3.91895E-04
5	1.22051E-01	2.08022E-01	2.19255E-01	2.20910E-01	2.30671E-01	2.24595E-01	2.17390E-01	2.21085E-01	2.17625E-01
6	0.	0.	0.	0.	0.	0.	0.	0.	0.
7	0.	0.	0.	0.	0.	0.	0.	0.	0.
ZEILEN 7 BIS 15 SIND GLEICH									
16	0.	0.	0.	0.	0.	0.	0.	0.	1.17315E-04
17	1.11701E-01	2.00735E-01	2.09909E-01	1.51210E-01	1.60587E-01	1.54071E-01	1.48328E-01	1.63959E-01	1.50311E-01
18	0.	1.02901E-02	7.20921E-03	8.76096E-03	6.83039E-02	6.74355E-02	6.66978E-02	6.81710E-02	3.31255E-02
19	0.	0.	1.91955E-08	5.28825E-10	0.	0.	0.	0.	0.
20	0.	0.	0.	0.	3.20676E-10	0.	0.	0.	0.
21	0.	0.	0.	0.	0.	1.94352E-10	0.	0.	0.
22	0.	0.	0.	0.	0.	0.	1.17878E-10	0.	0.
23	0.	0.	0.	0.	0.	0.	0.	1.14860E-10	0.
24	0.	0.	0.	0.	0.	0.	0.	0.	0.
ZEILEN 26 BIS 35 SIND GLEICH									

	SPALTE 11	SPALTE 12	SPALTE 13	SPALTE 14	SPALTE 15	SPALTE 16	SPALTE 17	SPALTE 18	SPALTE 19
1	4.39608E-04	6.25526E-04	2.51364E-03	4.99815E-03	3.80762E-03	2.20871E-03	2.22860E-03	3.11685E-03	9.63245E-03
2	2.13408E-01	2.07513E-01	2.10753E-01	2.14736E-01	2.13369E-01	2.12356E-01	2.14597E-01	2.29999E-01	2.51997E-01
3	7.44200E-03	1.07621E-03	3.99019E-03	8.09910E-03	6.18698E-03	3.33063E-03	3.17633E-03	4.29763E-03	7.65944E-03
4	1.08730E-03	1.60709E-03	6.86416E-03	1.38924E-02	1.07163E-02	5.86434E-03	5.76311E-03	7.96668E-03	1.43219E-02
5	2.24970E-01	2.18749E-01	2.21446E-01	2.25142E-01	2.23428E-01	2.21164E-01	2.22181E-01	2.29853E-01	2.32024E-01
6	6.16466E-04	5.99700E-04	5.44172E-03	1.17270E-02	8.28879E-03	4.59309E-03	6.56868E-03	5.91544E-03	7.48202E-03
7	0.	0.	0.	0.	0.	0.	0.	0.	0.
ZEILEN 7 BIS 10 SIND GLEICH									
11	0.	6.27103E-10	1.05085E-08	0.	0.	0.	0.	0.	0.
12	0.	9.15540E-09	6.60966E-08	6.63577E-08	0.	0.	0.	0.	0.
13	0.	4.22497E-07	1.06487E-06	4.62442E-07	1.74111E-06	0.	0.	0.	0.
14	0.	1.57345E-05	4.44133E-05	9.11481E-06	1.54203E-05	1.05905E-04	0.	0.	0.
15	0.	1.35360E-04	1.03960E-03	2.19880E-04	1.14778E-04	4.49743E-04	7.17736E-04	0.	0.
16	5.99700E-04	5.44172E-03	1.15916E-02	7.23346E-03	4.32837E-03	6.44371E-03	5.49175E-03	6.65656E-03	0.
17	1.38809E-01	1.80557E-01	1.45647E-01	1.32284E-01	1.54230E-01	1.84445E-01	1.98079E-01	2.15662E-01	2.16883E-01
18	4.03051E-02	7.75260E-02	2.47371E-02	2.69186E-02	4.17493E-02	4.16155E-02	2.53269E-02	1.56716E-02	3.97845E-03
19	5.46376E-07	4.22276E-03	4.19045E-04	5.43433E-03	2.16936E-02	2.38846E-02	9.01485E-03	6.29239E-03	1.68612E-03
20	0.	0.	0.	4.84245E-05	4.18102E-03	1.30073E-02	6.57232E-03	3.76300E-03	1.17686E-03
21	0.	0.	0.	0.	3.10546E-05	1.82213E-03	2.17401E-03	1.58906E-03	3.20787E-04
22	0.	0.	0.	0.	0.	0.	2.73732E-04	5.92220E-04	1.36018E-04
23	0.	0.	0.	0.	0.	0.	0.	6. 7679E-05	6.65378E-05
24	0.	0.	0.	0.	0.	0.	0.	0.	1.48060E-06
25	0.	0.	0.	0.	0.	0.	0.	0.	0.
ZEILEN 29 BIS 35 SIND GLEICH									

Table (8) HTR Leu 2 - Material 2

```
 4030220     HTR REFLECTOR 300K                                                    03.11.80

IMM=   35   IGM=   19   IMT=    5   IMS=   17   K1(5)=    0   K1(6)=    0   K1(7)=  665   K1(8)= 0446070002656077737 2

K1(9)=  0.            K1(10)=    0   L1=   298

      SPALTE   1   SPALTE   2   SPALTE   3   SPALTE   4   SPALTE   5   SPALTE   6   SPALTE   7   SPALTE   8   SPALTE   9

   1  0.           0.           0.           0.           0.           0.           0.           0.           0.
   2  1.980009E-01 3.577736E-01 3.785296-01 3.786726-01 3.788856-01 3.788946-01 3.789016-01 3.789086-01 3.798106-01
   3  2.660740E-05 5.978256-09 2.277116-06 5.870326-06 7.532326-06 9.666866-06 1.242616-05 1.813246-05 2.635196-05
   4  0.           0.           0.           0.           0.           0.           0.           0.           0.
   5  2.219666-01 3.820816-01 4.010536-01 4.013676-01 4.013796-01 4.013886-01 4.013946-01 4.014016-01 4.024016-01
   6  0.           0.           0.           0.           0.           0.           0.           0.           0.
   7  0.           0.           0.           0.           0.           0.           0.           0.           0.
  ZEILEN    7 BIS    15 SIND GLEICH
  16  0.           0.           0.           0.           0.           0.           0.           0.           2.198016-04
  17  2.028926-01 3.606316-01 3.847176-01 2.739786-01 2.752536-01 2.763676-01 2.741916-01 3.397086-01 2.775036-01
  18  0.           1.904746-02 1.345026-02 1.633406-02 1.273826-01 1.261186-01 1.256116-01 1.271916-01 6.167526-02
  19  0.           0.           0.           0.           0.           0.           0.           0.           0.
  ZEILEN   19 BIS   35 SIND GLEICH

      SPALTE  11   SPALTE  12   SPALTE  13   SPALTE  14   SPALTE  15   SPALTE  16   SPALTE  17   SPALTE  18   SPALTE  19

   1  0.           0.           0.           0.           0.           0.           0.           0.           0.
   2  1.815866-01 3.624416-01 3.634606-01 3.641286-01 3.648576-01 3.677686-01 3.922316-01 4.193436-01 4.552916-01
   3  4.389636-05 5.905546-05 7.598316-05 8.397936-05 9.244036-05 1.120046-04 1.426946-04 2.013036-04 3.585176-04
   4  0.           0.           0.           0.           0.           0.           0.           0.           0.
   5  4.032296-01 4.034016-03 4.035026-01 4.035946-01 4.036636-01 4.041916-01 4.063496-01 4.169396-01 4.174966-01
   6  1.128006-03 1.104216-03 1.002436-02 2.163996-02 1.930366-02 8.462676-03 1.204756-02 1.078536-02 1.332576-02
   7  0.           0.           0.           0.           0.           0.           0.           0.           0.
  ZEILEN    7 BIS    9 SIND GLEICH
  10  0.           1.211706-10 0.           0.           0.           0.           0.           0.           0.
  11  0.           1.176796-09 1.990746-08 0.           0.           0.           0.           0.           0.
  12  0.           1.717846-08 1.240376-07 1.247596-07 0.           0.           0.           0.           0.
  13  0.           7.931306-07 1.997036-06 8.677766-07 3.272026-06 0.           0.           0.           0.
  14  0.           2.953236-05 8.315406-05 1.709696-05 2.518476-05 1.991456-04 0.           0.           0.
  15  0.           2.530116-04 1.934006-03 4.094666-04 2.148056-04 8.404486-04 1.346866-03 0.           0.
  16  1.184216-03 1.002436-02 2.138696-02 1.334006-02 7.969256-03 1.181356-02 9.918676-03 1.177626-02 0.
  17  8.560126-01 3.341906-01 2.698566-01 2.460726-01 2.866726-01 3.423516-01 3.623486-01 4.008316-01 4.038126-01
  18  9.001506-02 1.451166-01 4.599686-02 4.980816-02 7.721286-02 7.701236-02 8.927986-02 2.865116-02 7.121446-03
  19  1.023986-06 7.910186-03 7.809176-04 1.015896-02 4.035216-02 4.373446-02 2.691106-02 1.177636-02 3.159716-03
  20  0.           0.           0.           9.183026-05 7.830686-03 2.814046-02 1.235856-02 7.069366-03 2.208526-03
  21  0.           0.           0.           0.           5.819046-05 3.415516-03 4.082266-03 2.236336-03 6.025216-04
  22  0.           0.           0.           0.           0.           0.           5.131616-04 1.037066-03 2.558146-04
  23  0.           0.           0.           0.           0.           0.           0.           1.238596-04 1.249656-04
  24  0.           0.           0.           0.           0.           0.           0.           0.           2.776976-06
  25  0.           0.           0.           0.           0.           0.           0.           0.           0.
  ZEILEN   25 BIS   35 SIND GLEICH
```

Table (9) HTR Reflector-Material 3

Iteration Number	k_{eff}	k_{eff} error	Max.Rel.Point Flux deviation
1	3.813053E+0	7.38E-1	1.50E+4
2	1.027808E+0	2.71E+0	2.91E+2
3	6.314833E-1	6.28E-1	2.87E+1
4	7.549026E-1	1.63E-1	-8.07E+0
5	8.618629E-1	1.24E-1	2.17E+0
6	9.069265E-1	4.97E-2	6.47E-1
7	9.239355E-1	1.84E-2	-4.65E-1
8	9.310134E-1	7.60E-3	-6.00E-1
9	9.34599E-1	3.84E-3	-8.80E-1
10	9.368233E-1	2.37E-3	-2.09E+0
11	9.383904E-1	1.67E-3	2.67E+0
16	9.429147E-1	1.70E-4	-2.77E-1
17	9.431306E-1	2.29E-4	-1.70E-1
22	9.432230E-1	1.55E-6	-1.34E-2

Table (10) PROTEUS-19 Group case. 18 Linear triangular elements. Ten iterations were required to estimate the dominance ratio $\sigma = .7546 \pm .038$. Coarse mesh rebalancing on throughout. Lebedev extrapolation with cycle length six switched on after the tenth iteration.

Iteration Number	k_{eff}	k_{eff} error	Max.Rel.Point Flux deviation
1	3.813053E+0	7.38E-1	1.50E+4
2	2.278383E+0	6.74E-1	-5.84E+1
3	2.351700E+0	3.12E-2	-1.82E+1
4	2.088541E+0	1.26E-1	5.08E+0
5	1.960709E+0	6.52E-2	-2.80E+0
6	1.829166E+0	7.19E-2	-4.02E+0
7	1.726901E+0	5.92E-2	1.42E+0
8	1.637616E+0	5.45E-2	5.28E-1
9	1.562142E+0	4.83E-2	2.90E-1
10	1.496698E+0	4.37E-2	1.74E-1
11	1.439960E+0	3.94E-2	-1.44E-1
16	1.243139E+0	2.46E-2	-3.36E-1
17	1.215773E+0	2.25E-2	-4.57E-1
22	1.114746E+0	1.47E-2	3.74E-1
23	1.099918E+0	1.35E-2	2.57E-1
28	1.043603E+0	8.88E-3	-1.16E-1
29	1.035142E+0	8.17E-3	-1.18E-1
34	1.002602E+0	5.39E-3	-1.39E-1

Table (11) PROTEUS-19 Group case. 18 Linear Triangular elements. Both, Lebedev extrapolations and coarse mesh rebalancing switched off.

Iteration Number	k_{eff}	k_{eff} error	Max.Rel.Point Flux Deviation
1	3.813053E+0	7.38E-1	1.50E+4
2	1.027808E+0	2.71E+0	2.91E+2
3	6.314833E-1	6.28E-1	2.87E+1
4	7.549026E-1	1.63E-1	-8.07E+0
5	8.618629E-1	1.24E-1	2.17E+0
6	9.069265E-1	4.97E-2	6.47E-1
7	9.239355E-1	1.84E-2	-4.65E-1
8	9.310134E-1	7.60E-3	-6.01E-1
9	9.345995E-1	3.84E-3	-8.80E-1
10	9.368233E-1	2.37E-3	-2.09E+0
11	9.383904E-1	1.67E-3	2.67E+0
16	9.420115E-1	4.11E-4	-3.06E-1
17	9.423055E-1	3.12E-4	-3.03E-1
21	9.429220E-1	1.03E-4	-2.79E-1

Table (12) Proteus-19 Group case. 18 Linear Triangular elements. Only coarse mesh rebalancing switched on.

Iteration Number	k_{eff}	k_{eff} error	Max.Rel.Point Flux deviation
1	3.813053E+0	7.38E-1	1.50E+4
2	2.278383E+0	6.74E-1	-5.84E+1
3	2.351700E+0	3.12E-2	-1.82E+1
4	2.088541E+0	1.26E-1	5.08E+0
5	1.960709E+0	6.52E-2	-2.80E+0
6	1.829166E+0	7.19E-2	-4.02E+0
7	1.726901E+0	5.92E-2	1.42E+0
8	1.637616E+0	5.45E-2	5.28E-1
9	1.562142E+0	4.83E-2	2.90E-1
10	1.496698E+0	4.37E-2	1.74E-1
11	1.439960E+0	3.94E-2	-1.44E-1
16	1.192367E+0	2.59E-2	-1.89E+1
17	7.156629E-1	6.66E-1	3.17E+1
22	-1.772160E+1	2.33E-1	-3.51E+2
23	-1.599682E+1	1.08E-1	9.81E+3
28	-6.787647E+0	1.75E-1	-1.07E+1
29	-5.568387E+0	2.19E-1	3.02E+2
34	-2.234791E+0	1.74E-1	-6.57E+0

Table (13) Proteus-19 Group case. 18 Linear Triangular elements. Ten iterations were required to estimate the dominance ratio $\sigma = .8942 \pm .04$, without using the coarse mesh rebalancing. A six cycle Lebedev extrapolation was switched on after the tenth iteration.

IHM denotes the length of the table i.e. the number of cross-sections specified for a given material in a specific group. IGM indicates the total number of groups, IHT and IHS the position, (the row label), containing the total and the self scatter cross sections, respectively.

Tables (10), (11), (12) and (13) display the results. Table (10) displays the results for the case where both the coarse mesh rebalancing scheme and the Lebedev extrapolation are activated. Ten iterations are required to estimate the dominance ratio to within $\pm$ 5 % and during this time only the coarse mesh rebalancing scheme is active. Thereafter, both the six cycle Lebedev and the rebalancing are active. Only the first and the last iteration of a particular cycle are displayed. Table (10) is used as a reference. Tables (11), (12) and (13) display identical iterations, whenever possible, for the sake of comparison.

The dominance ratio, σ, is a property of the iteration matrix. The result from Table (5) indicates $\sigma = .7546 \pm 0.038$ and Table (13) indicates $\sigma = .8942 \pm 0.04$. In practice the dominance ratio is computed via the flux which is the solution. Table (13) reflects a situation where no precautions are taken to ensure that the system is in neutronic balance. The rebalancing has greatest beneficial corrective effect on the upscattering which is predominant in this example. These, scattering sources are corrected, in Tables (10) and (12) and hence the difference in the estimated σ. The de-stabilizing effect of the Lebedev extrapolations in the absence of neutronic balance may also be noted. Table (11) displays the results of the situation where neither the rebalancing nor the extrapolations are in operation. It is to be noted that the convergence is very slow, but still, no instability results. Table (12) displays the results with only the coarse mesh rebalance active.

Unfortunately, the run terminated one iteration short. Comparing Tables (11) and (12) we see that the error in the k_{eff} reduces by a factor of approximately 0.92 every iteration, or by 0.66 over a cycle of six iterations in the absence of neutronic balance and by a factor of approximately 0.76 per iteration i.e. 0.25 for a cycle of six iterations when neutronic balance obtains. Note that these numbers correspond within a tolerance of $\pm$ 5 % to the dominance ratios estimated in Table (10) and (13).

The reason for discussing this problem at any length was to demonstrate the importance of the coarse mesh rebalancing in the presence of strong upscatter.

Example 4. 2D-IAEA Benchmark problem for L.W. reactors

This problem is an X-Y problem and has been discussed in detail in (1). It is a two group problem with no upscattering. Figs. (8) and (9) display the error in average power against the number of iterations for a cubic and a fourth order approximation with and without the Lebedev extrapolation. No coarse mesh rebalancing was used. In both cases the standard 9x9 mesh which results in sixty nine triangular elements was used - vide Fig. (13) in reference (1). The benefit of the Lebedev extrapolations is evident. The inclusion of coarse mesh rebalancing brings no additional tangible improvements. This is due to the absence of upscattering. The rebalancing, as implimented here, brings most benefit when upscatter is present.

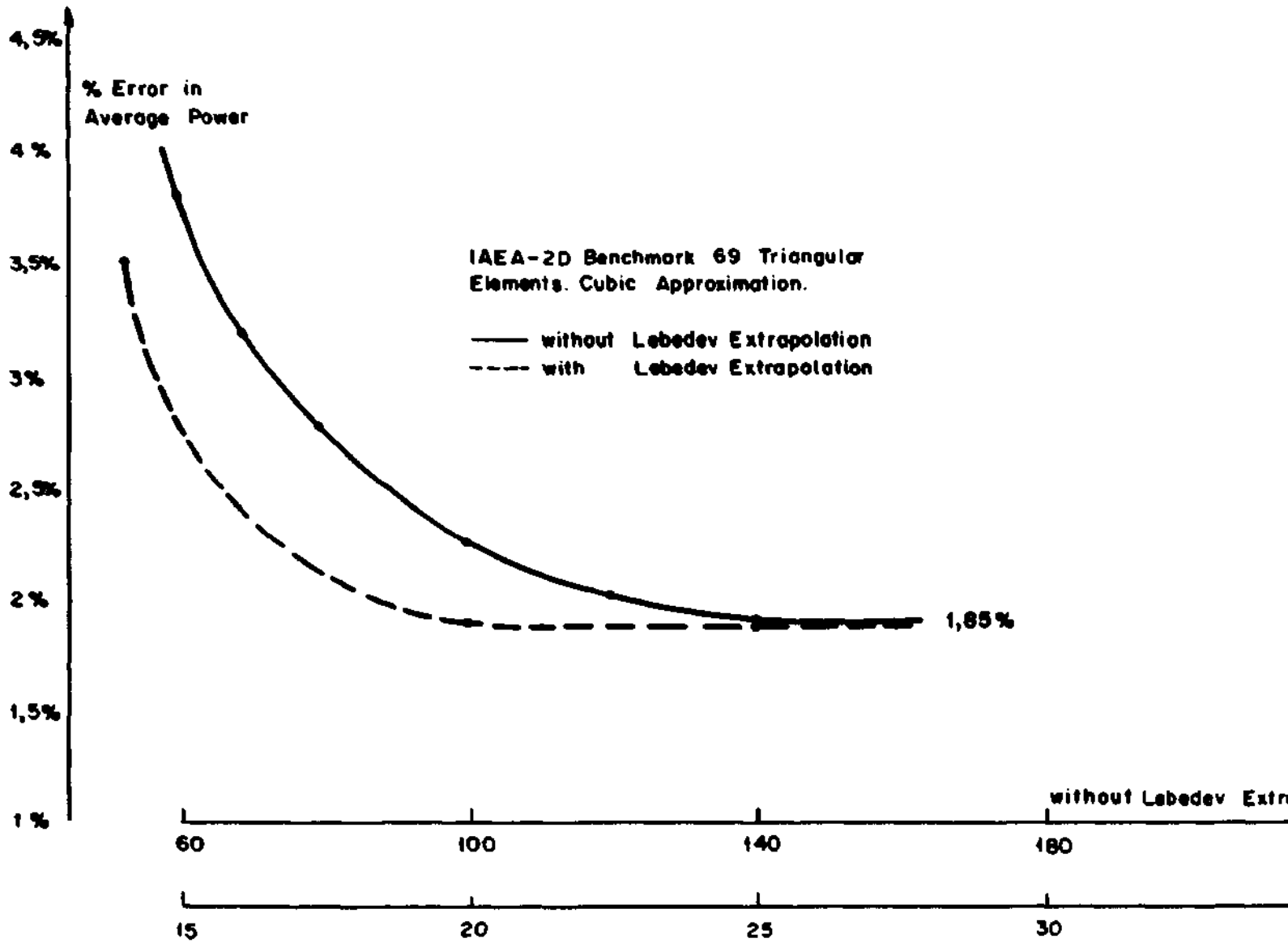
4,5%
% Error in
Average Power
4 %
3,5%
3%
2,5%
2 %
1,5%
1 %
IAEA-2D Benchmark 69 Triangular
Elements. Cubic Approximation.
without Lebedev Extrapolation
with Lebedev Extrapolation
1,85%
without Lebedev Extr
60
100
140
180
15
20
25
30
with Lebedev Extrapo

Fig. (8)

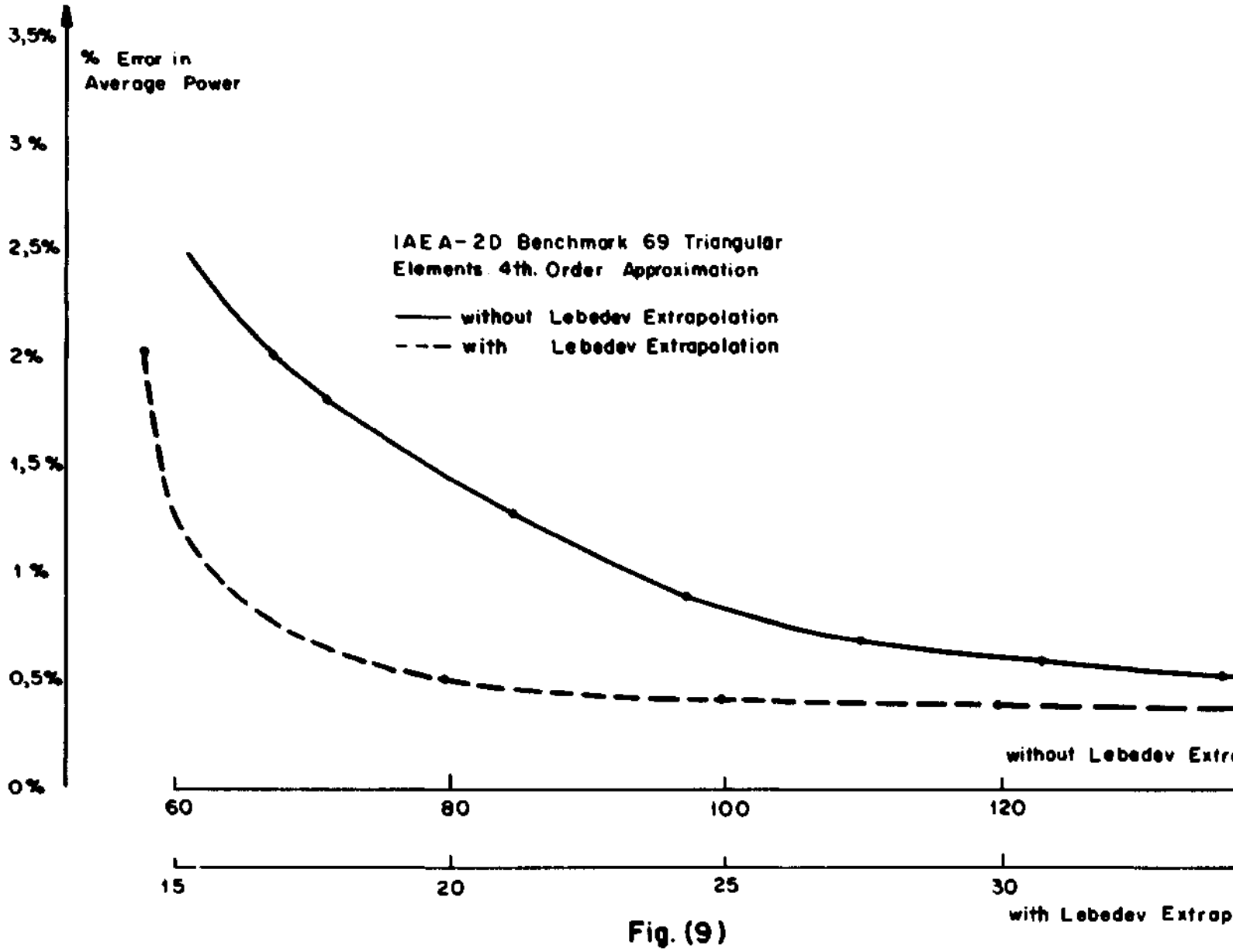
3,5%
% Error in
Average Power
3 %
2,5%
2%
1,5 %
1 %
0,5%
0%
IAEA-2D Benchmark 69 Triangular
Elements 4th. Order Approximation
without Lebedev Extrapolation
with Lebedev Extrapolation
60
80
100
120
without Lebedev Extr
15
20
25
30
with Lebedev Extrap

Fig. (9)

References

1) Davierwalla-"FINELM: a multigroup finite element diffusion code. Part I - X-Y geometry and dissections" - EIR report 419, Dez. 1980

2) Davierwalla-"A finite element solution to the neutron diffusion equation in two dimensions" - ISNM 37 Birkhäuser Verlag, 1977.

3) Lebedev and Finogenov-"Ordering of the iterative parameters in the cyclical Chebyshev iterative method". USSR Comput. Math. and Math.Phys.II (2) 1971 (155-170)

4) Lebedev and Finogenov-"Solution of the parameter ordering problem in Chebyshev iterative methods". - USSR Comput.Math.and Math.Phys. 13 (1), 1973 (21-41)

5) Varga, R.-"Matrix Iterative Analysis" Prentice Hall

6) Benchmark Book - Argonne National Research Lab-ANL 7416